JGR Space Physics

RESEARCH ARTICLE
10.1029/2023JA032137

Surface Charging of the Jupiter Icy Moons Explorer (JUICE) Spacecraft in the Solar Wind at 1 AU

M. K. G. Holmberg[1], C. M. Jackman[1], M. G. G. T. Taylor[2], O. Witasse[2], J.-E. Wahlund[3,4], S. Barabash[5], B. Michotte de Welle[6], H. L. F. Huybrighs[1], C. Imhof[7], F. Cipriani[2], G. Déprez[2], and N. Altobelli[8]

[1]School of Cosmic Physics, DIAS Dunsink Observatory, Dublin Institute for Advanced Studies, Dublin, Ireland, [2]ESTEC, European Space Agency, Noordwijk, The Netherlands, [3]Swedish Institute of Space Physics, Uppsala, Sweden, [4]Department of Physics and Astronomy, Uppsala University, Uppsala, Sweden, [5]Swedish Institute of Space Physics, Kiruna, Sweden, [6]LPP, CNRS, Ecole Polytechnique, Sorbonne Universite, Institut Polytechnique de Paris, Palaiseau, France, [7]Airbus Defence and Space GmbH, Immenstaad, Germany, [8]ESAC, European Space Agency, Madrid, Spain

Abstract This article presents the first study of the interaction between the Jupiter Icy Moons Explorer (JUICE) spacecraft and the solar wind environment at 1 AU. The state-of-the-art software Spacecraft Plasma Interaction Software was used to simulate the surface charging of the spacecraft and the altered particle environment around the spacecraft. The simulations show that for a typical solar wind environment the spacecraft will charge to around 6 V, with the different dielectric parts of the spacecraft charging to potentials from around −36 to 8 V. For the studied extreme solar wind environment, similar to the environment found in the sheath region inside the shock front of an Interplanetary Coronal Mass Ejection, the surface potential of the spacecraft is lower due to the increased accumulation of electrons. The spacecraft will charge to around 3 V, with the different dielectric surfaces charging from around −45 to 9 V. We also show how the interaction between the spacecraft and its environment alters the ion and electron particle environment around the spacecraft. This study is the first step toward developing correction techniques for the impact that the interaction between the JUICE spacecraft and its environment has on the JUICE charged particle and field measurements.

Plain Language Summary All spacecraft interact with their space environment. This interaction can create a variety of different problems, with a severity that depends on the environment and the design of the spacecraft. Here, we present a study of the interaction between the Jupiter Icy Moons Explorer (JUICE) spacecraft and the solar wind environment at 1 AU. We study both a typical solar wind environment and an extreme environment, for example, the environment encountered during an Interplanetary Coronal Mass Ejection. Our simulations show that we can expect the different parts of the spacecraft to charge from around −45 to 9 V. The interaction between JUICE and the solar wind will also alter the particle environment around the spacecraft. We present the altered charged particle environment around the spacecraft, both for the ion and the various electron populations. This study is the first step toward developing correction techniques for the impact that the interaction between the JUICE spacecraft and its environment has on the JUICE measurements.

Key Points:

- The interaction between the Jupiter Icy Moons Explorer spacecraft and the solar wind environment at 1 AU, is simulated
- We present the spacecraft surface potentials, typically ranging from −45 to 9 V, for different solar wind conditions
- We also present the near spacecraft particle environment, which is altered due to the interaction between the spacecraft and its environment

Supporting Information:

Supporting Information may be found in the online version of this article.

Correspondence to:

M. K. G. Holmberg,
mika.holmberg@pm.me

Citation:

Holmberg, M. K. G., Jackman, C. M., Taylor, M. G. G. T., Witasse, O., Wahlund, J.-E., Barabash, S., et al. (2024). Surface charging of the Jupiter Icy Moons Explorer (JUICE) spacecraft in the solar wind at 1 AU. *Journal of Geophysical Research: Space Physics*, *129*, e2023JA032137. https://doi.org/10.1029/2023JA032137

Received 3 OCT 2023
Accepted 13 AUG 2024

1. Introduction

In this study we investigate the surface charging of the Jupiter Icy Moons Explorer (JUICE) spacecraft in the solar wind near Earth, using the Spacecraft Plasma Interaction Software (SPIS) version 6.1.0. Surface charging can have a substantial impact on particle and field measurements and an extensive understanding of the charging and its impact is therefore crucial for the particle and field data analysis. The aim of this work is to provide a detailed study of the surface charging of JUICE in the solar wind at 1 AU in order to support the analysis of the JUICE measurements. This environment is of particular interest since the first JUICE particle and field observations was recorded in the solar wind at 1 AU. It therefore provides the first opportunity to compare simulation results with observations and to start using the simulation results as a tool to improve the data analysis. JUICE will also spend a substantial amount of time in this environment, during the first half of the cruise phase of the mission, so additional observations will be available.

Due to the complexity of the problem, surface charging is best studied using numerical models. There are several suites of spacecraft charging simulation software available, but for this study we use the state-of-the-art software SPIS, which is also used by the European Space Agency (ESA) to study the impact of spacecraft charging on their

missions. SPIS is used to model the interaction between a spacecraft and its space environment. SPIS was initiated in 2001 by ESA, supported by the French National Centre for Space Studies (CNES), and developed in collaboration with the French Aerospace Laboratory (ONERA) and Artenum. The software is an open-source Java based hybrid code package that can handle both a kinetic treatment of the particle populations, using a Particle-In-Cell (PIC) method, and a fluid treatment. SPIS is used to resolve electrostatic spacecraft—plasma interactions. A more detailed description of SPIS can be found in Sarrailh et al. (2015). The SPIS simulation set-up requires one to define a spacecraft geometry model, a computational mesh, the spacecraft material properties, the internal circuitry, and the simulated space environment.

SPIS has previously been used to study the surface charging and its impact on missions like Rosetta (e.g., Bergman et al., 2020b; Sjögren et al., 2012), Parker Solar Probe (Diaz-Aguado et al., 2021a; Guillemant et al., 2012), Solar Orbiter (Guillemant et al., 2017), and Cassini (Holmberg et al., 2021). Here we present the first study of the surface charging of JUICE in the solar wind at 1 AU. Several studies have also shown the significant impact surface charging can have on the spacecraft's charged particle and field measurements, see, for example, Engwall et al. (2006); Bergman et al. (2020a, 2020b); Holmberg et al. (2021); Diaz-Aguado et al. (2021b) and Bochet et al. (2023). Engwall et al. (2006) studied the ion wake formation behind a spacecraft, which occurs when the relative speed between the spacecraft and the plasma flow is larger than the thermal energy of the ions. This will result in the ions not being able to fill up the space behind the spacecraft and a depletion of ions, called an ion wake, is formed. Engwall et al. (2006) showed that for a positively charged spacecraft the potential structure around the spacecraft can act as the obstacle to the positive ions instead of the spacecraft itself. This occurs when the kinetic energy of the positive ions is not sufficient to overcome the potential barrier and the ions then scatter on the potential structure instead of the spacecraft surface. Hence, careful consideration of the extension of the ion wake is needed for accurate ion measurement analysis, so that a depletion in ions is not assumed to be a natural phenomena when in fact it is due to the positively charged spacecraft. Bergman et al. (2020a, 2020b) studied the impact surface charging has on charged particle measurements, both the effect on the energy and the direction of travel of the particles, for the Ion Composition Analyzer (RPC-ICA) on the Rosetta spacecraft. They showed that the low-energy particle measurements were heavily distorted by the surface charging of the spacecraft but that the distortion is strongly dependent on the viewing direction of the instrument. This was further elaborated in Bochet et al. (2023), who studied the impact of surface charging on the JUICE Jovian plasma Dynamics and Composition (JDC) analyzer measurements in the Jovian magnetosphere and the ionosphere of Jupiter's moon Ganymede. They correlated the simulated ion measurement distortions for different viewing directions of JDC to the charging of different parts of the JUICE spacecraft, such as the solar panels and the JUICE magnetometer boom (J-MAG). The studies by Bergman et al. (2020a, 2020b) and Bochet et al. (2023) were all focused on positive ion measurements, but the same methods can also be used to study the impact on electron and negative ion measurements. Holmberg et al. (2021) used SPIS to study the ion wake formation of the Cassini spacecraft and showed that Langmuir probe ion measurements in the wake can differ with one order of magnitude from the ambient ion density, which stresses the importance of a detailed knowledge of the ion wake structure for accurate data analyses. Holmberg et al. (2021) also showed how detailed knowledge of the ion wake structure can be used to constrain plasma parameters, such as the ion temperature, when accurate measurements are not available. The examples listed above states a few of the different ways that the interaction between a spacecraft and its environment can impact the spacecraft measurements. These examples are also relevant for the JUICE measurements.

This study provides the basic parameters, such as the surface potential of the spacecraft, needed to provide accurate corrections to the data to compensate for the impact the spacecraft - environment interaction will have on the JUICE particle and field measurements in the solar wind at 1 AU. The results from this study are therefore of crucial importance to future studies focused on developing correction techniques for the JUICE particle and field measurements.

2. Simulation Set-Up

2.1. JUICE and Its Instruments

The JUICE mission is a large-class ESA mission with the aim of studying the Jovian system, its formation, and the habitability of the icy moons of Jupiter. The spacecraft was launched on 14 April 2023 and will arrive at Jupiter in 2031. In 2034, JUICE will go into orbit around Ganymede, and will then become the first spacecraft to ever orbit a moon other than the Earth's. After 9 months in orbit around Ganymede the spacecraft is planned to be disposed of,

for planetary protection reasons, by an impact with Ganymede. JUICE is carrying 10 instrument packages, which will be used to study Jupiter and the Jovian system in greater detail than ever before. The two main instrument packages that are targeting charged particle and field observations are the Radio and Plasma Wave Investigation (RPWI) package and the Particle Environment Package (PEP), which will be used to study the plasma environments in the Jovian system. In addition, the J-MAG is used to make in-situ observations of the local magnetic field. The J-MAG observations are not suspected to be impacted by the charging of JUICE in the studied solar wind environments. Our simulations show currents to and from the spacecraft of the order of 1 mA, which is estimated to produce magnetic fields that are smaller than the 1 pT noise level of J-MAG. The J-MAG measurements are therefore not further discussed in this article.

JUICE also carries various other instruments whose measurements will most likely not be directly affected by spacecraft charging, but which are referred to in the description of the spacecraft model. These instruments are: the Ganymede Laser Altimeter (GALA) that will study the topography of the icy moons; the optical camera system (JANUS) that will be used to study the morphology and processes on Jupiter's moons and perform mapping of Jupiter's clouds; the Moons and Jupiter Imaging Spectrometer (MAJIS) that will study the atmospheric constituents on Jupiter and characterize the icy moon surfaces; the Radar for Icy Moons Exploration (RIME) that will be used to study the subsurface structures of the icy moons; the Sub-millimeter Wave Instrument (SWI) that will characterize Jupiter's atmosphere, and the exospheres and surfaces of the icy moons; the UV imaging spectrograph (UVS) that will be used to study the exospheres of the icy moons and the upper atmosphere and aurorae of Jupiter; and the Gravity and Geophysics of Jupiter and the Galilean Moons (3GM) that will be used to study Ganymede's gravity field, the oceans of Jupiter's icy moons, and the atmosphere of Jupiter. JUICE will also use the standard telecommunication system to perform the Planetary Radio Interferometer and Doppler Experiment (PRIDE).

In order to perform the SPIS simulations we have used a detailed spacecraft model, presented in Figure 1. Panel a, b, c, and d shows the −x, x, z, and −z sides of the spacecraft, respectively. The notation of the different sides of the spacecraft refers to the spacecraft coordinate system, where

- x is in the opposite direction of the high-gain antenna (HGA)
- y is along the solar panels
- z completes the right hand system

The spacecraft model consists of a main body of $2.25 \times 2.50 \times 3.52$ m, a high-gain antenna (HGA) with a radius $r_{\mathrm{HGA}} = 1.27$ m, and solar panels that extend 7.44 m in the z direction and 12.07 m in the y direction. The model contains most of the instruments and radiators. Figure 1 also includes the four RPWI Langmuir probes (LPs), with the locations of LP1 and LP4 marked as they are used to discuss the simulation results in Section 3. The LPs are, however, not included in the simulations since their inclusion would increase the simulation time but not alter the results presented in this article. This is because the LPs have conductive surfaces and a negligible total surface area compared to the rest of the spacecraft. Figure 1c also shows the location of the PEP Jovian Electrons and Ions (JEI) instrument as it is also used to discuss the simulation results in Section 3. As a first approach, the JUICE solar panels have been simulated as equipotential surfaces without any exposed biased elements. The inclusion, exclusion, and modification of the various parts of the spacecraft and its instruments have been carefully considered with the aim of decreasing simulation time and memory use without losing accuracy. This has been studied in detail by running multiple simulations including various smaller parts of the spacecraft and by varying the surface materials and their properties. The color coding used in Figure 1 refers to the following surface materials and spacecraft parts:

- Gray: Black Kapton, spacecraft body, UVS, J-MAG, PEP/JDC
- Black: Indium tin oxide (ITO) coating, solar panels
- White: White paint Z93C55, HGA, radiators
- Green: White paint PSG 120 FD coated with ITO, PEP card rack radiator
- Brown: Electrodag 501, GALA, PEP/Jovian Neutrals Analyzer (JNA)
- Blue: Enbio SolarBlack, MLI around main engine, thrusters
- Yellow: Gold equivalent, PEP/Neutral gas and Ion Mass spectrometer (NIM), PEP/Jovian Energetic Neutrals and Ions (JENI)
- Red: Steel, Medium Gain Antenna (MGA), SWI, main engine nozzle

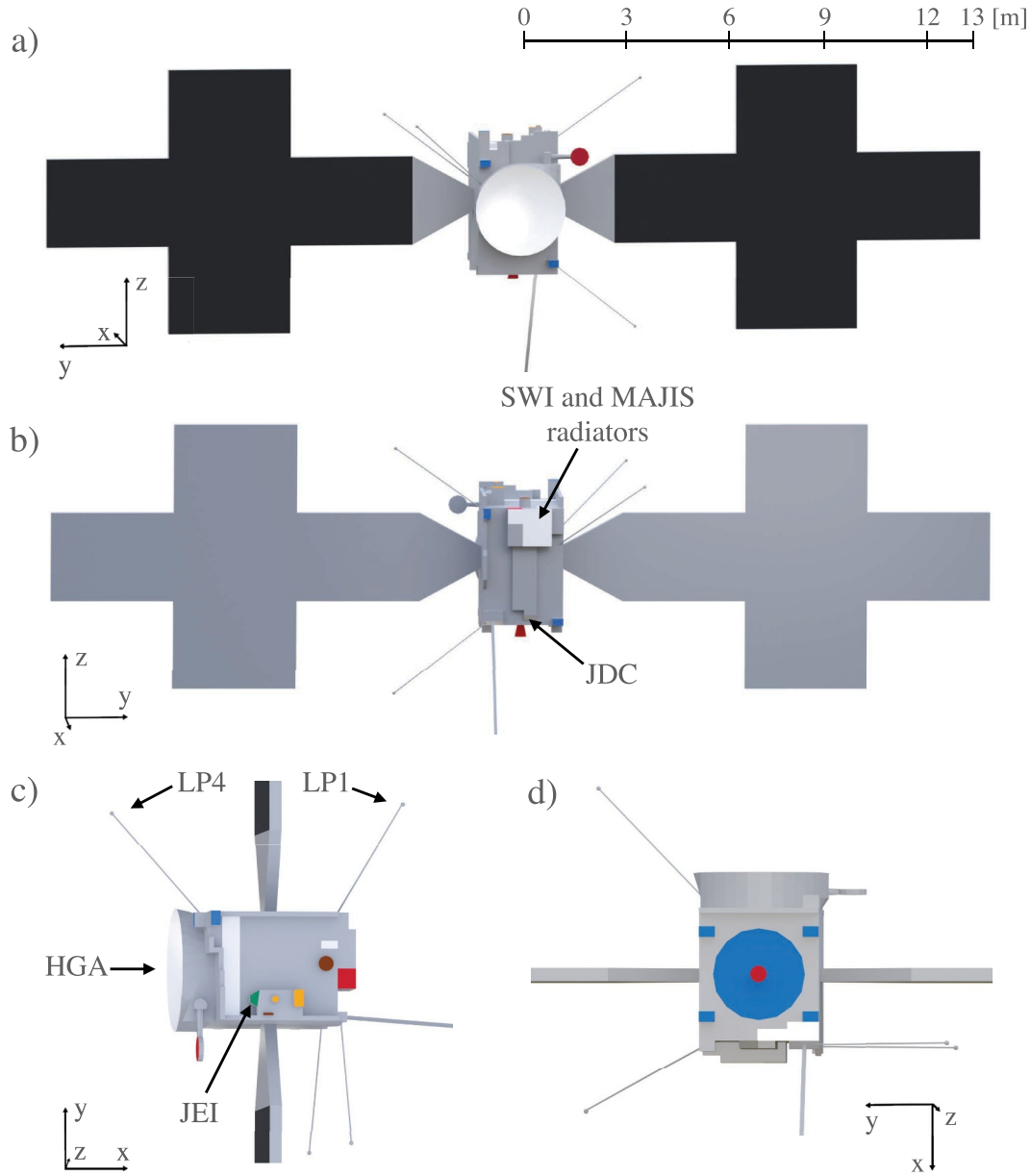

Figure 1. (a) The -x side of the spacecraft model showing the HGA (white), the medium-gain antenna (MGA) (red) and the ITO covered solar panels (black). (b) The x side of the spacecraft showing the SWI and MAJIS radiators (white), thrusters (blue) and the back of the solar panels covered in black Kapton (gray). The arrows locate the SWI and MAJIS radiators and the PEP/JDC instrument. (c) The z side of the spacecraft showing the top vault radiator (white), various instruments of PEP (yellow and green), GALA (brown), and SWI (red). The arrows locate the HGA, the PEP/Jovian Electrons and Ions (JEI) instrument and two of the RPWI Langmuir probes, LP1 and LP4. (d) The -z side of the spacecraft showing the MLI around the main engine and thrusters (blue), the bottom vault radiator (white) and the main engine nozzle (red). To reduce simulation times, the spacecraft model does not include the RIME antenna.

The only dielectric material included in the simulations is the white paint Z93C55, which is covering the white surfaces in Figure 1. The material properties used to simulate this paint is listed in Table S1 in the Supporting Information. The applied paint is between 75 and 100 μm thick for all the Z93C55 covered surfaces that are included in the above spacecraft model. A small sensitivity study showed that the choice of paint thickness, 75 or 100 μm, will not affect the surface potentials generated in the studied environments. For the simulations presented in this article, a Z93C55 paint thickness of 75 μm was used.

Since the material properties of PSG 120 FD are readily available in the SPIS material library, this paint has been used for the PEP card rack radiator instead of the SG 121 FD paint that is actually covering the radiator. Both paints are silicate based paints doped with zinc oxide (ZnO) and they are expected to have the same material properties. In addition, the surface is covered in a nm-thick ITO layer and grounded, and the paint has therefore been simulated as conductive. Using PSG 120 FD instead of SG 121 FD will have a negligible impact on the final simulation results, due to the similarities between the two materials, the small area of the radiator and the conductive surface material.

2.2. The Solar Wind Near Earth

The first JUICE measurements were performed in the solar wind near Earth during the Near Earth Commissioning Phase (NECP). The NECP extended from 15 April until 15 July 2023. The measurements were recorded when JUICE was located in between 1,500 and 3,200 Earth radii (1 R_E = 6,378 km) from Earth. The trajectory of JUICE from launch until the end of the NECP is illustrated in Figure 2, which shows that the spacecraft is located in the undisturbed solar wind, far from Earth's magnetosphere, when the measurements were recorded.

In order to simulate the interaction between the spacecraft and its environment we need to know the properties of the ambient solar wind. We have obtained the properties from various solar wind studies, further discussed in the next few paragraphs. The values of the environment parameters used for the simulations are presented in Tables 1 and 2. Column 1 of Tables 1 and 2 gives the parameter's name, column 2 gives the used value, column 3 states the values obtained from different data sets and studies, and column 4 gives the references for the values given in column 3. The values listed in column 3 includes mean values and ranges, when both are stated the range is given within parentheses after the mean value.

The solar wind electrons are simulated as two populations, the core (cold) and halo (hot) electrons. The third solar wind electron population, the strahl electrons, typically has densities that are only a few percent of the core electron density (Štverák et al., 2009). The strahl electron population provides therefore no significant contribution to the surface charging of the spacecraft and is not included in the simulations. The core and halo electron densities $n_{e,c}$ and $n_{e,h}$, and temperatures $T_{e,c}$ and $T_{e,h}$, are obtained from the studies listed in Table 1 column 3. The core and halo electrons are simulated using Maxwellian and Kappa distributions, respectively.

To describe the typical solar wind, we use mean values for the ion density n_i, the solar wind velocity v_{sw}, and the magnetic field strength $|B|$, obtained from the data set presented in Michotte de Welle et al. (2022). The data set, hereafter referred to as M1, consists of measurements from Cluster, Double Star, Themis, and MMS performed between 2001 and 2021 (Michotte de Welle et al., 2022). We have obtained the magnitude of the mean solar wind velocity, $|v_{sw}|$, from the M1 data set. The solar wind is set to travel in the x direction in the spacecraft coordinate system, that is, the solar wind will be hitting the front of the spacecraft, shown in Figure 1a. From the M1 data we

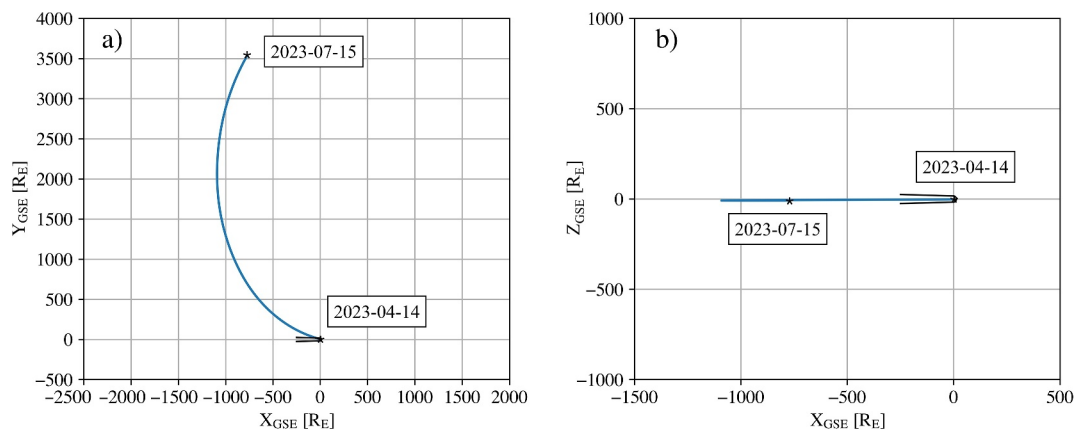

Figure 2. The JUICE trajectory (blue), in Geocentric Solar Ecliptic (GSE) coordinates, from launch on 14 April 2023 to the end of NECP on 15 July 2023. The black line outlines the magnetosphere of Earth, with the Sun toward the right. Panel (a) shows the trajectory in the XY plane, which is the plane of Earth's orbit around the Sun, seen from above the north pole and panel (b) gives the trajectory in the XZ plane, so seen from the side. The black stars mark the beginning and end of the trajectory.

Table 1
Environmental Parameters Describing the Typical Solar Wind

Parameter	Input value	Reference values	References
$n_{e,c}$	5.4 cm^{-3}		Assuming $n_{e,c} + n_{e,h} = n_i$
$T_{e,c}$	10 eV	10, 12.2, 10, 8.5–10	Gosling (2014), Wilson et al. (2018), Lazar et al. (2020), Pierrard et al. (2020)
$n_{e,h}$	0.2 cm^{-3}	0.2, 0.2–0.3, 0.2	Maksimovic et al. (2005), Lazar et al. (2020), Pierrard et al. (2020)
$T_{e,h}$	60 eV	60, 60–66	Lazar et al. (2020), Pierrard et al. (2020)
Kappa	5	4.9, 4.5–5, 5–5.7, 5–5.5	Maksimovic et al. (2005), Štverák et al. (2009), Lazar et al. (2020), Pierrard et al. (2020)
n_i	5.6 cm^{-3}	5.6, 6.4 (0.03–72), 6 (0.5–117)	M1, M2, Venzmer and Bothmer (2018)
T_i	8 eV	8, 4.3–10.3, 12.7, 9	M2, Gosling (2014), Wilson et al. (2018),Venzmer and Bothmer (2018)
$\lvert v_{sw}\rvert$	413 km/s	413, 427, 468, 410 (156–1,189)	M1, M2, Gosling (2014), Venzmer and Bothmer (2018)
Ion species	H^+		
$v_{s/c,x}$	−1.0 km/s		From the spacecraft trajectory file Crema 5.0b23.1
$v_{s/c,y}$	−33 km/s		
$v_{s/c,z}$	−0.04 km/s		
$\lvert B\rvert$	5.5 nT	5.5, 5.7, 6.2, 6 (0.4–62)	M1, M2, Gosling (2014), Venzmer and Bothmer (2018)

have also obtained the magnitude of the mean interplanetary magnetic field (IMF), $|B|$. The IMF is set to the y direction in the spacecraft coordinate system.

The values from the M1 data set have also been compared with the results from Venzmer and Bothmer (2018). They used hourly OMNI data from 1963 to 2016 to present the frequency distribution of proton temperature, and solar wind density, velocity, and magnetic field strength. The two data sets are in very good agreement, despite being recorded by different spacecraft. The values from the M1 data set are also in very good agreement with mean values obtained from OMNI data from 1995 to 2021, this data set is referred to as M2. This time interval was chosen in order to compare the mean values from the data set presented in Michotte de Welle et al. (2022), that is, the mean values from the M1 data set, with measurements from the ACE and WIND spacecraft only.

The parameters listed in Table 1 describe the mean solar wind that JUICE will interact with. In order to study a larger range of possible interactions, between JUICE and the solar wind, we also study the interaction under "extreme" solar wind conditions, for example, the conditions that have been observed in Interplanetary Coronal Mass Ejection (ICME)-driven shocks. Observations of ICMEs at 1 AU show that the shock is typically characterized by a sharp increase in solar wind velocity, density, ion temperature, and magnetic field strength (Carcaboso et al., 2020; Kilpua et al., 2017). It is therefore reasonable to assume that the environment with the highest solar wind density is also the environment with the largest velocity, and highest ion temperature and magnetic field strength. We have used the maximum values for these parameters (except for the solar wind velocity), presented in Venzmer and Bothmer (2018), to describe the extreme solar wind environment found in the sheath regions of ICMEs. Using the highest solar wind velocity of 1,189 km/s would require an unnecessary long simulation time since the particles will move through the computational volume too fast and therefore require an extremely small simulation time step. This velocity is also much higher than what is typically detected within the shock front of ICMEs. We therefore use a somewhat lower, but still high, solar wind velocity of 700 km/s. The extreme solar wind is set to travel in the x direction and the extreme IMF is set to the y direction in the spacecraft coordinate system, just like for the typical solar wind environment. The values of the parameters used for the extreme solar wind environment simulation are listed in Table 2.

Newbury et al. (1998) showed an electron temperature increase of around a factor 1.5 following an interplanetary shock. We have therefore chosen a core electron temperature of 15 eV for the extreme solar wind environment.

Laboratory measurements of photoelectron emission from various commonly used spacecraft materials show that the photoelectron distributions typically are Maxwellian with a temperature ranging from 1.2 to 1.5 eV (Grard, 1973). We have therefore used a Maxwellian photoelectron distribution with a temperature of 1.3 eV for both the typical and extreme solar wind environments. We have used the PIC method to simulate the ion and electron populations for both the typical and extreme solar wind environments.

Table 2
Parameters Describing the Extreme Solar Wind Environment Created by, for Example, ICME-Driven Shocks

Parameter	Input value	Reference values	References
$n_{e,c}$	116.8 cm^{-3}		Assuming $n_{e,c} + n_{e,h} = n_i$
$T_{e,c}$	15 eV[a]	10, 12.2, 10, 8.5–10	Gosling (2014), Wilson et al. (2018), Lazar et al. (2020), Pierrard et al. (2020)
$n_{e,h}$	0.2 cm^{-3}	0.2, 0.2–0.3, 0.2	Maksimovic et al. (2005), Lazar et al. (2020), Pierrard et al. (2020)
$T_{e,h}$	60 eV	60, 60–66	Lazar et al. (2020), Pierrard et al. (2020)
Kappa	5	4.9, 4.5–5, 5–5.7, 5–5.5	Maksimovic et al. (2005), Štverák et al. (2009), Lazar et al. (2020), Pierrard et al. (2020)
n_i	117 cm^{-3}	5.6, 6.4 (0.03–72), 6 (0.5–117)	M1, M2, Venzmer and Bothmer (2018)
T_i	571 eV	8, 4.3–10.3, 12.7, 9 (0.3–571)	M2, Gosling (2014), Wilson et al. (2018), Venzmer and Bothmer (2018)
$\lvert v_{sw} \rvert$	700 km/s	413, 427, 468, 410 (156–1,189)	M1, M2, Gosling (2014), Venzmer and Bothmer (2018)
Ion species	H^+		
$v_{s/c,x}$	−1.0 km/s		From the spacecraft trajectory file Crema 5.0b23.1
$v_{s/c,y}$	−33 km/s		
$v_{s/c,z}$	−0.04 km/s		
$\lvert B \rvert$	62 nT	5.5, 5.7, 6.2, 6 (0.4–62)	M1, M2, Gosling (2014), Venzmer and Bothmer (2018)

[a]The core electron temperature is 1.5 times the reference value (Newbury et al., 1998).

For this study we did not take into account the variability of the solar UV flux, but simply used the reference values provided by SPIS. As a first approach, this is deemed sufficient. However, the importance of the variable solar UV flux should be considered when simulating the actual measurements, as it might have an impact on the final surface potentials for the situations where the photoelectron currents are driving the charging of the spacecraft.

3. Results and Discussion

3.1. Interaction in the Typical Solar Wind

The SPIS simulations provide a variety of information that will be important for the analysis of the future measurements of JUICE. The main result is the surface charging of the spacecraft, illustrated in Figure 3. Figure 3 shows that the spacecraft body and the solar panels (spacecraft ground) will charge up to ∼6 V and the surfaces covered in the dielectric material (the white paint Z93C55) will reach different potentials. The most positively charged surface is the HGA which will reach a potential of ∼8 V. The HGA is directed toward the Sun and the solar wind, which is causing the emission of photoelectrons and accumulation of ions to have a larger impact on the charging of the HGA, compared to the rest of the spacecraft. The spacecraft model also includes several of the radiators that are covered with Z93C55. They are all shielded from the solar radiation by sun shields or different parts of the spacecraft and will therefore charge negatively. The most negatively charged surface is the bottom vault radiator, which reached a potential of ∼−36 V. However, the potentials of the Z93C55 surfaces should be used with care since the material properties for this paint is not as well constrained as the ones for the conductive surfaces of the spacecraft. The bottom vault radiator is not producing any photoelectrons, as it is shielded from the Sun, but does still accumulate solar wind electrons. This, in combination with a negligible accumulation of solar wind ions, is charging the surface negatively. The same reasoning applies to the other radiators that are also charging to negative potentials. The potentials would be different if the spacecraft obtained a different orientation relative to the Sun and solar wind, however, within around 1.3 AU the HGA needs to act as a sun shield in order to maintain a healthy temperature of the spacecraft. The orientation of the spacecraft relative to the Sun and the solar wind will therefore be the simulated one during all parts of the mission when the spacecraft is within 1.3 AU, except for a few short instances when, for example, spacecraft rolls are needed for instrument calibrations.

Figure 4, panels a to c, show the density of the different particle populations around the spacecraft along three lines starting from the center of the spacecraft and crossing the positions of two of the RPWI/Langmuir probes (panels a and b) and the PEP/JEI instrument (panel c). The figures show the photoelectron density (dashed line), the ion density (dotted line), the core electron density (solid line) and the halo electron density (dashdotted line).

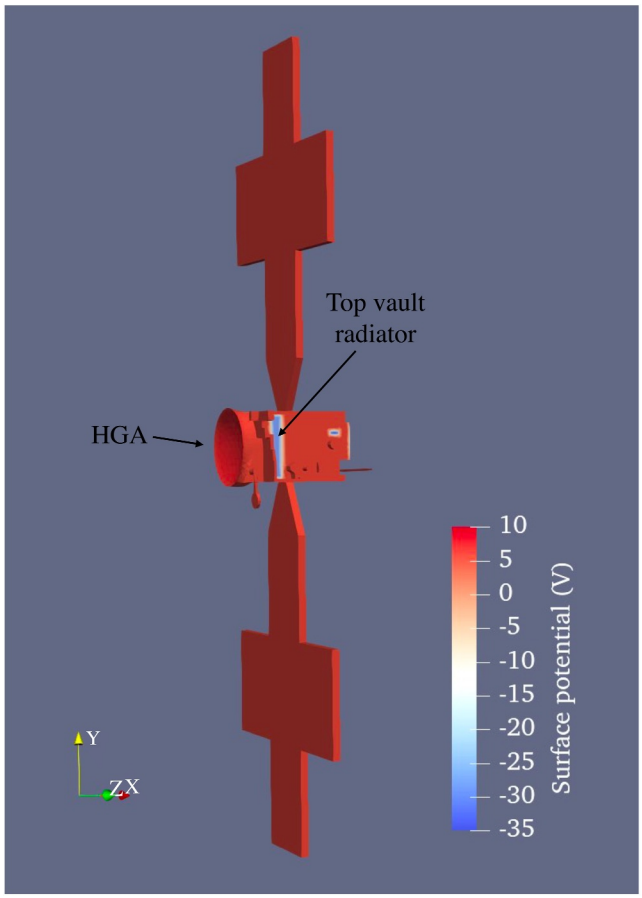

Figure 3. The simulated surface potential of JUICE for the mean solar wind environment. The spacecraft will charge to ~6 V and the HGA, which is a dielectric surface and is pointing directly toward the Sun as it acts as a sun shield for this part of the mission, will charge to around ~8 V. The radiators, which are also dielectric, will charge to potentials between −26 and −36 V. The difference in potentials are due to the locations of the surfaces relative to the Sun and solar wind. The arrows locate the HGA and the top vault radiator.

The vertical black lines of panels a and b mark the positions of LP1 (panel a), which is located on the back of the spacecraft and LP4 (panel b), which is located on the front of the spacecraft, see Figure 1c. The JEI instrument is located at x = 0 in Figure 4c. Figure 4, panels a to c, show that the spacecraft will be surrounded by a thick photoelectron cloud with densities much higher than the solar wind density, which is due to the close proximity to the Sun during this part of the mission and the typically low solar wind density. In fact, the photoelectron density close to the sunlit surface of the spacecraft, the -x side of the spacecraft, will reach up to more than 130 times the solar wind density (not shown). The produced photoelectrons starts to gyrate around the local magnetic field and are typically attracted back to the spacecraft, since the spacecraft is positively charged, and are therefore also present behind the spacecraft. The photoelectron density on the back of the spacecraft (positive x direction), close to the JDC instrument, is closer to 2 times the solar wind density. Figure 4, panels a and b, show particle densities on the y side of the spacecraft and panel c shows the densities around the JEI instrument, which is located on the z side of the spacecraft, see Figure 1c. Hence, even though the instruments are not located on the sunlit surface of the spacecraft, the dominant, or one of the main, particle density at all three instruments is the photoelectron density. This needs to be taken into consideration when performing the data analysis for these instruments. The densities around LP2 and LP3, located on the -y side of the spacecraft (see Figure 1), are very similar to the results for LP1 (panel a) and are therefore not shown.

It is important to point out that for the LP measurements there will also be contributions from the photoelectrons and secondary electrons produced by the probes themselves (see e.g., Holmberg et al., 2012, 2017; Wang et al., 2015), which are not considered in the presented simulations as it is beyond the scope of this study. However, based on the results presented in Figures 4a and 4b, it is reasonable to assume that they will provide significant contributions to the currents measured by the LP in the typical solar wind environment and also needs to be properly corrected for.

Figure 4d shows the potential along lines starting from the center of the spacecraft and crossing the positions of LP1 (black and the same line as the densities presented in panel a are recorded along), LP4 (blue and line of panel b) and the JEI instrument (red and line of panel c). The surface of the spacecraft is set to x = 0. The LPs will be used to measure electric fields under the assumption that the potential field around the spacecraft is symmetric. Figure 4d shows that the potential, however, can differ by more than one V for the same distance from the surface, which needs to be corrected for in order to obtain accurate electric field measurements.

The potential asymmetry is caused by both the use of materials with different material properties and the spacecraft's asymmetric geometry. Figure 4d shows that the potential along line LP1 (black) falls of faster than the potentials along lines LP4 (blue) and JEI (red). This is due to the close proximity of line LP1 to the MAJIS and SWI radiators that are located on the back of the spacecraft, shown in Figure 1b. These radiators are charged to negative potentials and are impacting the local spacecraft potential field. For the same reason, the line starting at the location of the JEI instrument (red) is decreasing faster due to its close proximity to the top vault radiator, shown in Figure 3. This, however, is only a local effect that is noticeable up to around 0.2 m from the spacecraft surface as the negative potential of the top vault radiator is suppressed by the positive potential of the rest of the spacecraft. Outside of this local effect, the potential along the JEI line is falling off slower than the potential along the LP4 line due to the asymmetric geometry of the spacecraft.

Figure 5a shows a cross-section of the ion density around the spacecraft, with the ion wake clearly outlined. The ions are not able to fill up the space behind the spacecraft if the relative speed between the plasma and the spacecraft is larger than the thermal speed of the ions, which is causing the depletion of ions shown in Figure 5a.

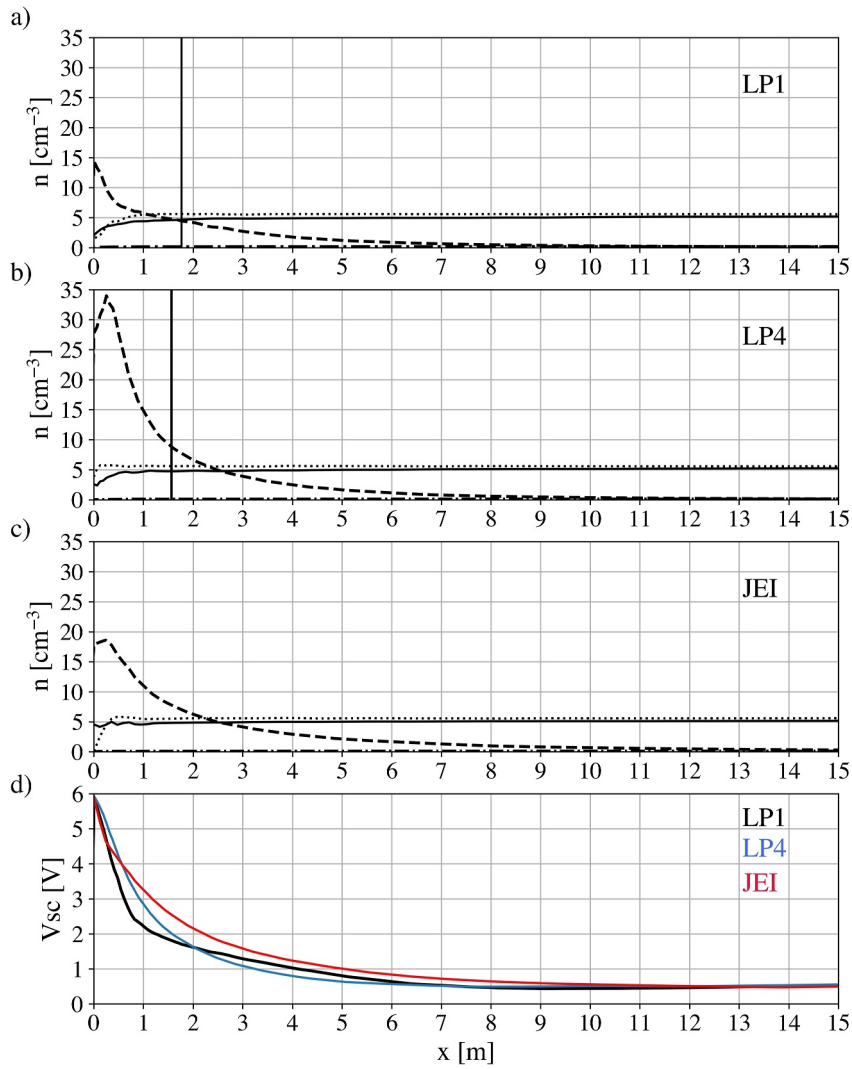

Figure 4. The figure shows the particle densities and potentials from the typical solar wind environment simulations. (a) The particle densities around the spacecraft following a line starting at the center of the spacecraft and reaching 15 m from the surface of the spacecraft, which is set to 0. The line crosses the location of LP1 (black vertical line), which is located on the opposite side of the HGA (see Figure 1c). The figure shows the photoelectron density (dashed line), the ion density (dotted line), the core electron density (solid line), and the halo electron density (dashdotted line). (b) The particle densities along a 15 m line that crosses the position of LP4 (black vertical line), which is located on the same side as the HGA (see Figure 1c). The various particle populations are the same as in panel a. (c) Same outline as in panel a and b but along a line that crosses the position of the PEP/JEI instrument, located at x = 0. (d) The potentials along a 15 m line that crosses the locations of LP1 (black), LP4 (blue) and the JEI instrument (red).

The ion density is reduced to close to 0 cm^{-3} at the x side surface of the spacecraft. Hence, the PEP/JDC instrument, which is located on the x side of the spacecraft (see Figure 1b) will not be able to measure solar wind ions with this spacecraft attitude, which will be the default spacecraft attitude for the part of the mission when JUICE is within 1.3 AU. Figure 5a shows that the ion wake is a structure many times larger than the spacecraft itself. For example, at 65 m behind the spacecraft the ion density is reduced to 4 cm^{-3}, from a density of 5.6 cm^{-3} in the undisturbed solar wind.

Figure 5b shows the photoelectron density around the spacecraft. Figure 5b confirms the results shown in Figure 4, panels a to c, that the photoelectrons will be the dominant particle population around the spacecraft for the typical solar wind environment. The maximum photoelectron density, just above the surface of the solar panels, is 760 cm^{-3}. Since the spacecraft is charged positively and the photoelectrons are of just a few eV energy,

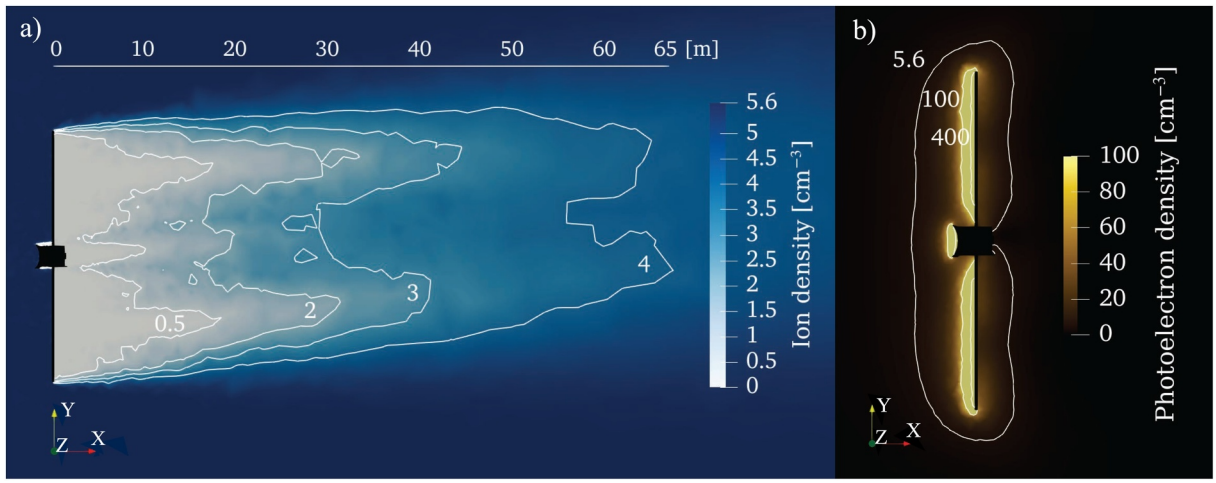

Figure 5. (a) A cross-section of the ion density in a xy plane cutting the center of the JUICE spacecraft, which is shown in black, in the typical solar wind environment. The ion wake is clearly outlined as the depletion of ions behind the spacecraft. The isolines (white) give the densities at 0.5, 2, 3, and 4 cm^{-3}. The Sun is toward -x and the solar wind is moving in the x direction. (b) The photoelectron density around the JUICE spacecraft for the typical solar wind environment. The isolines (white) outline the densities 5.6 (the solar wind density), 100, and 400 cm^{-3}.

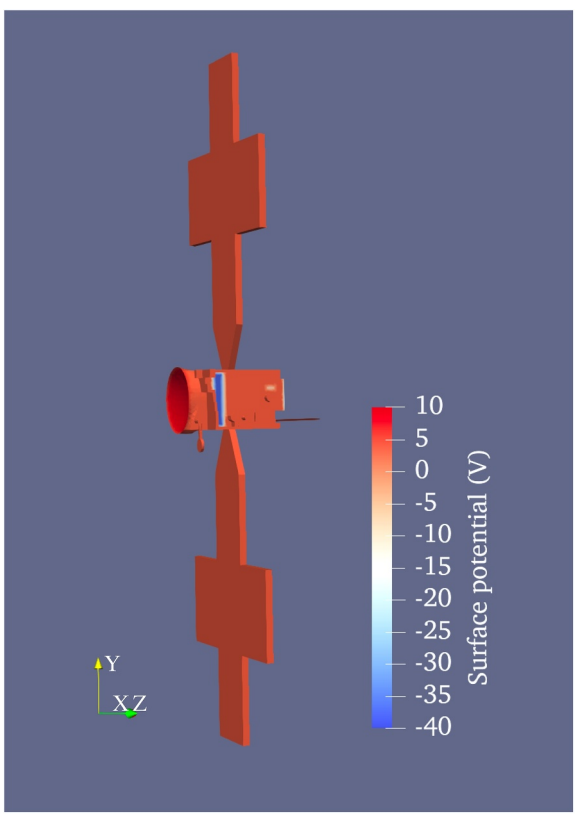

Figure 6. The surface potential of JUICE for the extreme solar wind environment. The spacecraft will charge to ~3 V, with the different dielectric surfaces reaching higher, ~9 V, or lower potentials, ~−45 V, depending on their orientation relative to the Sun and solar wind.

most photoelectrons will be attracted back to the spacecraft. This process also makes it possible for the photoelectrons to reach the spacecraft surfaces that are not in sunlight.

3.2. Interaction in the Extreme Solar Wind

The extreme solar wind environment is a much denser, hotter, and faster environment than the typical solar wind. This might, for example, describe the situation in the sheath inside the shock front of an ICME. This kind of environment will drive the spacecraft potential toward lower values due to the increase in accumulation of electrons. Figure 6 shows that the spacecraft body and the solar panels will charge up to around 3 V and the surfaces covered in the dielectric material (the white paint Z93C55) will reach different potentials. The most positively charged surface is the HGA, which will reach a potential of around 9 V. The HGA is directed toward the Sun and will have an even larger emission of photoelectrons and accumulation of ions, relative to the rest of the spacecraft. There are also several radiators painted with Z93C55, but they are all shielded from the solar radiation and will therefore have no production of photoelectrons. The radiators will charge to negative potentials, down to −45 V.

Figure 7, panels a to c, show the density of the different particle populations around the spacecraft along three lines starting from the center of the spacecraft and crossing the positions of two of the RPWI/Langmuir probes (panels a and b) and the PEP/JEI instrument (panel c). The set up is the same as for Figure 4, but the densities are the ones obtained for the extreme solar wind environment. The vertical black lines of panels a and b, which show the positions of LP1 and LP4, show that the dominant particle populations for this environment at the locations of the LPs are the solar wind electrons and ions. Figure 7 panels a to c also include the secondary electron density (thick black lines). This population is produced by the halo electrons that are interacting with the spacecraft surface and causing an emission of secondary electrons. The maximum density of this population is around 2 cm^{-3}, close to the

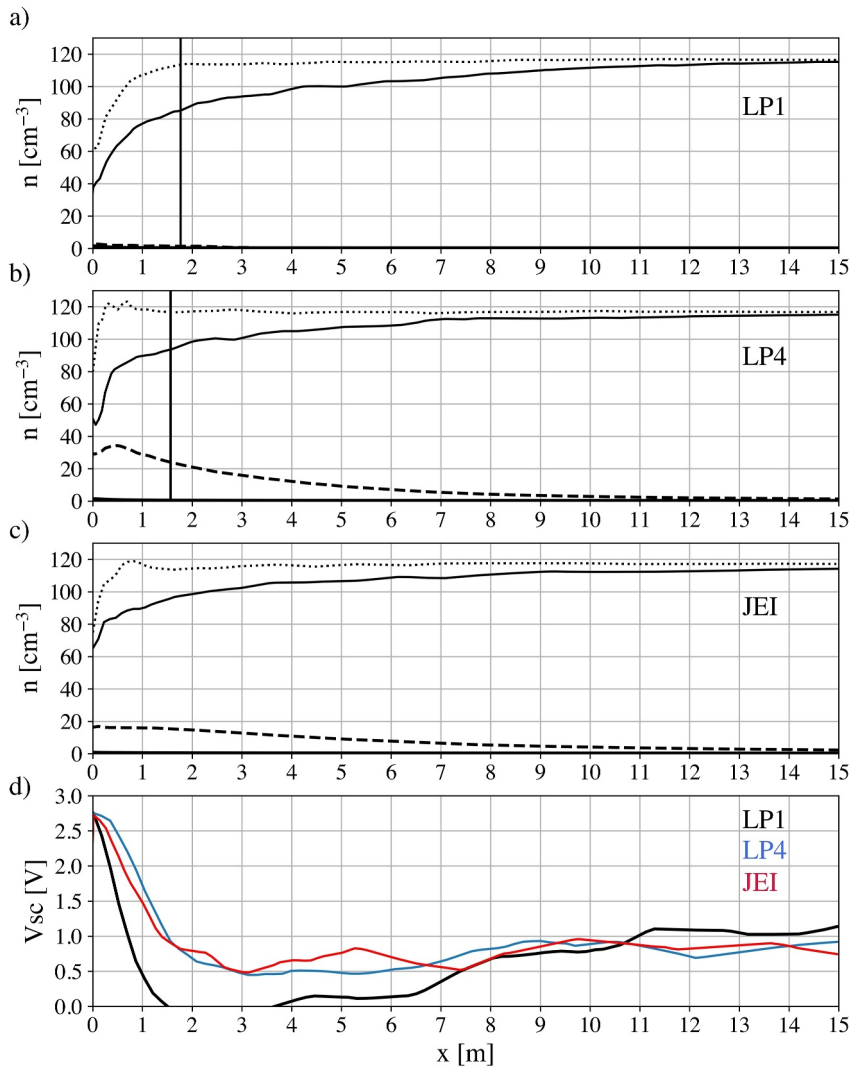

Figure 7. The figure shows the particle densities and potentials from the extreme solar wind environment simulations. (a) The particle densities around the spacecraft following a line starting from the center of the spacecraft and reaching 15 m from the surface of the spacecraft, which is set to 0. The line crosses the location of LP1 (black vertical line), which is located on the opposite side of the HGA (see Figure 1c). The figure shows the photoelectron density (dashed line), the ion density (dotted line), the core electron density (solid line), and the secondary electron density produced by the halo electrons (thick solid line). The secondary electron density has a maximum of only 2 cm^{-3} and is therefore hard to separate from the x-axis. (b) The particle densities along a 15 m line that crosses the position of LP4 (black vertical line), which is located on the same side as the HGA (see Figure 1c). The various particle populations are the same as in panel a. (c) Same outline as in panel a and b but along a line that crosses the position of the PEP/JEI instrument, located at x = 0. (d) The potentials along a 15 m line that crosses the locations of LP1 (black), LP4 (blue), and the JEI instrument (red).

surface of the spacecraft. At the positions of LP1 and LP4 this density is closer to 0.1–0.2 cm^{-3}. The secondary electron population, originating from the spacecraft body and produced by the halo electrons, should therefore only provide a negligible contribution to the currents measured by the LPs, for this environment. The various particle densities around LP2 and LP3, located on the -y side of the spacecraft (see Figure 1), are very similar to the results for LP1 (panel a) and are therefore not shown.

Figure 7d shows the potentials along three lines starting from the center of the spacecraft and crossing the locations of LP1 (black), LP4 (blue), and JEI (red). The surface of the spacecraft is set to x = 0. Figure 7d confirms the results from Figure 4d, that the potential structure around the spacecraft will be asymmetric. The asymmetric potential structure is, as noted in Section 3.1, due to the spacecraft's variety of materials and asymmetric geometry. For the extreme solar wind environment, an additional contribution to the potential along line LP1 (black)

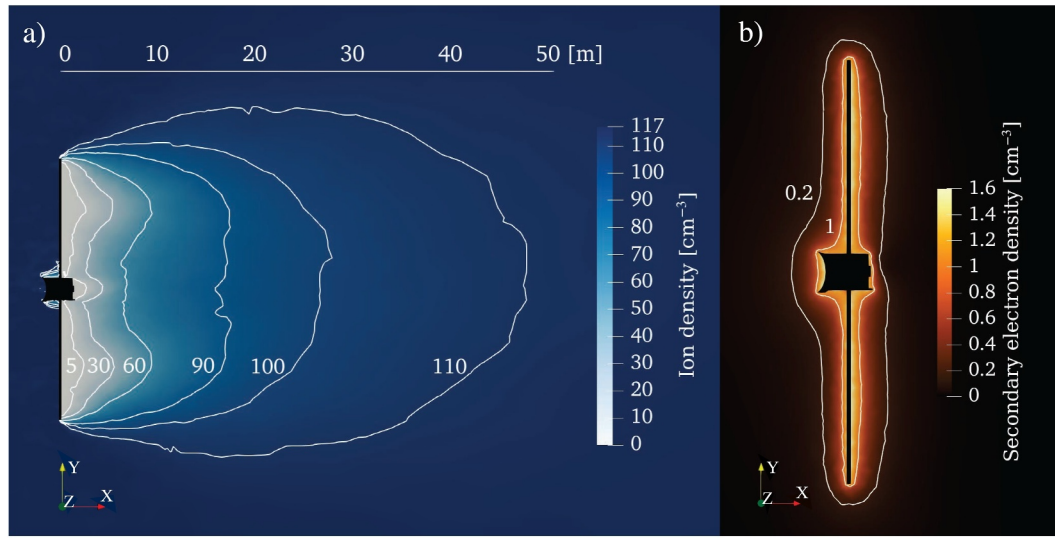

Figure 8. (a) A cross-section of the ion density in a xy plane cutting the center of the JUICE spacecraft, which is shown in black, in the extreme solar wind environment. The ion wake is clearly outlined as the depletion of ions behind the spacecraft. The isolines (white) give the densities at 5, 30, 60, 90, 100, and 110 cm^{-3}. The Sun is toward -x and the solar wind is moving in the x direction. (b) The secondary electron density around the JUICE spacecraft for the extreme solar wind environment. The isolines (white) outline the densities 0.2 and 1 cm^{-3}.

comes from the depletion of ions behind the spacecraft that creates a region of negative potential. The potential along line LP1 (black) reaches down to a minimum of −0.2 V at 2.4 m. This contribution is negligible for the potential along line LP1 in the typical solar wind environment since the typical solar wind density is lower and the spacecraft surface potential is higher.

Figures 6 and 7 show that the disturbances both from the potential of the spacecraft and the various particle populations originating from the spacecraft itself will be much smaller for the extreme solar wind environment than for the typical solar wind environment, since the spacecraft potential is lower and the particle densities of both the photoelectron densities and the secondary electron densities are much smaller than the solar wind density. It is important to point out that for the LP measurements there will also be a contribution from the photoelectrons and secondary electrons produced by the instrument itself, which are not included in the simulations presented here. However, based on the results presented in Figures 6 and 7 it is reasonable to assume that the current contributions to the JUICE LPs from these particle populations also will be small compared to the one from the ambient solar wind, for an extreme solar wind environment like the one studied here.

Figure 8a shows the ion density around the spacecraft for the extreme solar wind environment, with the ion wake clearly outlined behind the spacecraft. The isolines give the densities at 5, 30, 60, 90, 100, and 110 cm^{-3}. Figure 8b shows the secondary electron density around the spacecraft and the isolines give the densities at 0.2 and 1 cm^{-3}.

3.3. Outgassing and Its Impact on the Spacecraft Potential

Outgassing from the spacecraft was not taken into account in the simulations presented in Section 3.1 and 3.2. This is a process that could impact the charging of the spacecraft if the density of these particles is high enough. Spacecraft outgassing is the diffusion of gases from the surface and interior of a spacecraft, which will create a thin gas cloud around the spacecraft. Spacecraft outgassing is most prominent during the first few months after launch, but can occasionally be detected many years after launch. Spacecraft outgassing has been studied in detail by, for example, Schläppi et al. (2010). They used 6 years of the Rosetta Orbiter Spectrometer for Ion and Neutral Analysis (ROSINA) measurements recorded during the cruise phase of Rosetta. Rosetta was located between 0.88 and 2.2 AU and the solar panels were 64 m^2, hence comparable to the JUICE mission during the first part of the cruise phase. Schläppi et al. (2010) presented a neutral gas pressure of $\sim 4 \times 10^{-11}$ mbar, mainly due to desorbed water molecules, 60 days after launch. The neutral gas pressure decreased rapidly and stabilized to

$\sim 4 \times 10^{-10}$ mbar 200 days after launch. Using $P = n_{H2O} k_B T_{H2O}$, where P is the gas pressure, n_{H2O} is the water number density, k_B is the Boltzmann constant, and T_{H2O} is the water temperature, and assuming $T_{H2O} = 150$ K, we obtain water densities of 1.9×10^7 cm^{-3} and 1.9×10^6 cm^{-3}. With a photoionization rate of 8.28×10^{-7} s^{-1} at 1 AU (Huebner & Mukherjee, 2015) and an electron impact ionization rate of 8×10^{-8} s^{-1} at 1 AU (Cravens et al., 1987) we estimate that the charged particle density will be $\sim$18 cm^{-3} 60 days after launch and $\sim$1.8 cm^{-3} 200 days after launch. These densities are too low to contribute significantly to the charging of the spacecraft in the typical solar wind environment, where the charging is mainly driven by the large photoelectron production, and also in the extreme solar wind environment where the increased solar wind density will be the dominant driver of the charging of the spacecraft. Hence, outgassing from the JUICE spacecraft is not expected to contribute significantly to the charging of the spacecraft, but it will surely impact, and needs to be considered, for the neutral particle measurements in the early part of the mission when the outgassing is still substantial.

4. Conclusions

The results presented in this study show that the impact of spacecraft charging must be considered when analyzing the future cold plasma measurements performed by JUICE. The study is focused on the charging in the solar wind at 1 AU since this is where the first JUICE particle and field observations were recorded. This environment therefore provides the first opportunity to compare simulation results with observations and to start using the simulation results as a tool to improve the data analysis. We have shown that the JUICE spacecraft - plasma interaction will have a substantial impact on the charging of the spacecraft and on altering the particle environment around the spacecraft, both by the large production of photoelectrons from the spacecraft itself and the formation of an ion wake around the spacecraft.

For the typical solar wind environment at 1 AU, obtained from 20 years of spacecraft solar wind observations, our simulations indicate that JUICE will charge to around 6 V, with potentials for the various dielectric surfaces ranging from −36 to 8 V. This spacecraft surface potential is in very good agreement with the potential of 5 V that was measured during the first RPWI Langmuir probe sweep performed in the solar wind during the NECP (Wahlund et al., 2024). This surface potential will impact the cold plasma measurements of the particle analyzers JDC and JEI, both by distorting the particle trajectories and altering the energy of the surrounding particles (Bergman et al., 2020a, 2020b; Bochet et al., 2023), hence cold plasma measurements needs to be corrected for the impact of the potential of the spacecraft. Detailed SPIS simulations dedicated to each instrument and particle population are needed in order to provide the magnitude of the needed data corrections.

In the typical solar wind environment the spacecraft will be surrounded by a dense photoelectron cloud with a maximum density of up to 760 cm^{-3} close to the sunlit surface. The photoelectron densities at the locations of the four LPs will be between 5 and 10 cm^{-3} and around 20 cm^{-3} at the surface of the cold plasma instrument JEI. The potential structure around the spacecraft is shown to vary with more than one V for the same radial distance from the spacecraft, which needs to be taken into account when performing electric field measurements. An ion wake is formed behind the spacecraft and the depletion of ions can be detected more than 65 m away from the spacecraft. Typically the structure of the wake needs to be taken into consideration when analyzing Langmuir probe measurements, so that the decrease in ion density is not mistaken for a plasma depletion in the ambient solar wind. However, our simulations show that due to the orientation of the spacecraft and the locations of the Langmuir probes none of them are located within the ion wake for the studied cases. On the other hand, the PEP/JDC instrument is always located in the ion wake and will therefore not be able to perform solar wind ion observations unless the spacecraft attitude is altered, for example, during a spacecraft roll.

For the extreme solar wind, JUICE will charge to slightly lower potentials due to the increase in accumulation of electrons. The spacecraft body will reach a potential of around 3 V, with the different dielectric parts of the spacecraft charging to between −45 and 9 V. In the extreme solar wind environment the photoelectron cloud around the spacecraft is no longer the dominant particle population and minor interference with the LP measurements is expected. The potential structure around the spacecraft is confirmed to be asymmetric also for this environment. The asymmetry is due to the spacecraft's variety of materials, asymmetric geometry, and ion wake.

The relatively small difference in potential between the typical and the extreme solar wind environment simulations indicates that the surface potential of the spacecraft in the solar wind at 1 AU will be relatively stable. For the typical solar wind, the surface potential of the spacecraft is driven by the emission and absorption of photoelectrons, while the absorption of solar wind electrons and ions is of minor importance. Hence, the surface

potentials of the spacecraft will stay around 6 V even if the density of the solar wind decreases. This is the reason why we have not included a simulation using a low solar wind density environment. It is, however, possible that a large change in the electron temperatures would result in surface potentials outside of the presented range. But studies of solar wind electrons show surprisingly steady core and halo electron temperatures, even during large changes in solar wind velocity (Halekas et al., 2020; Pierrard et al., 2020). Consequently, the simulations presented in this article likely cover the surface potential ranges that the JUICE spacecraft will experience during most of the first part of its cruise phase. The JUICE spacecraft potential measurements, which will soon be available, will show if this assumption is correct.

The results of this study provide information that will be used when developing methods to correct the JUICE charged particle and field measurements, in the solar wind at 1 AU, accounting for the impact the interaction between the spacecraft and its environment will have. As discussed throughout the article, spacecraft charging affects particle and field measurements in various ways. Therefore, the next step in developing correction techniques will depend on the specific type of measurement being addressed. But generally, for a given measurement type and set of solar wind conditions, the next step would be to use SPIS to simulate these specific measurements. This approach will offer a detailed understanding of how the interaction between the JUICE spacecraft and its environment affect specific measurements, laying the groundwork for the needed data corrections.

Data Availability Statement

SPIS (Spacecraft Plasma Interaction Software, 2024) can be downloaded at https://www.spis.org/software/spis/get/. The spacecraft speed is obtained from (JUICE Operational SPICE Kernel Dataset, 2024) at https://doi.org/10.5270/esa-ybmj68p.

Acknowledgments
MKGH acknowledges support from the Science Foundation Ireland (Grant 18/FRL/6199) and the Discovery programme of the European Space Agency (Contract No: 4000137683/22/NL/GLC/my). CMJ's work at DIAS has been supported by the Science Foundation Ireland (Grant 18/FRL/6199). The authors would like to thank J. Cadavid for support with Figure 1.

References

Bergman, S., Stenberg Wieser, G., Wieser, M., Johansson, F. L., & Eriksson, A. (2020a). The influence of spacecraft charging on low-energy ion measurements made by RPC-ICA on Rosetta. *Journal of Geophysical Research: Space Physics*, *125*(1), e2019JA027478. https://doi.org/10.1029/2019JA027478

Bergman, S., Stenberg Wieser, G., Wieser, M., Johansson, F. L., & Eriksson, A. (2020b). The influence of varying spacecraft potentials and Debye lengths on in situ low-energy ion measurements. *Journal of Geophysical Research: Space Physics*, *125*(4), e2020JA027870. https://doi.org/10.1029/2020JA027870

Bochet, M., Bergman, S., Holmberg, M. K. G., Wieser, M., Stenberg Wieser, G., Wittmann, P., et al. (2023). Perturbations of JUICE/JDC ion measurements caused by spacecraft charging in the Jovian magnetosphere and the ionosphere of Ganymede. *Journal of Geophysical Research: Space Physics*, *128*(9), e2023JA031377. https://doi.org/10.1029/2023JA031377

Carcaboso, F., Gómez-Herrero, R., Espinosa Lara, F., Hidalgo, M. A., Cernuda, I., & Rodríguez-Pacheco, J. (2020). Characterisation of suprathermal electron pitch-angle distributions - Bidirectional and isotropic periods in solar wind. *Astronomy & Astrophysics*, *635*, A79. https://doi.org/10.1051/0004-6361/201936601

Cravens, T. E., Kozyra, J. U., Nagy, A. F., Gombosi, T. I., & Kurtz, M. (1987). Electron impact ionization in the vicinity of comets. *Journal of Geophysical Research*, *92*(A7), 7341–7353. https://doi.org/10.1029/JA092iA07p07341

Diaz-Aguado, M. F., Bonnell, J. W., Bale, S. D., Wang, J., & Gruntman, M. (2021a). Parker Solar Probe FIELDS instrument charging in the near Sun environment: Part 1: Computational model. *Journal of Geophysical Research: Space Physics*, *126*(5), e2020JA028688. https://doi.org/10.1029/2020JA028688

Diaz-Aguado, M. F., Bonnell, J. W., Bale, S. D., Wang, J., & Gruntman, M. (2021b). Parker Solar Probe FIELDS instrument charging in the near Sun environment: Part 2: Comparison of in-flight data and modeling results. *Journal of Geophysical Research: Space Physics*, *126*(5), e2020JA028689. https://doi.org/10.1029/2020JA028689

Engwall, E., Eriksson, A. I., & Forest, J. (2006). Wake formation behind positively charged spacecraft in flowing tenuous plasmas. *Physics of Plasmas*, *13*(6). https://doi.org/10.1063/1.2199207

Gosling, J. (2014). Chapter 12 - The solar wind. In T. Spohn, D. Breuer, & T. V. Johnson (Eds.), *Encyclopedia of the solar system* (3rd ed., pp. 261–279). Elsevier. https://doi.org/10.1016/B978-0-12-415845-0.00012-8

Grard, R. J. L. (1973). Properties of the satellite photoelectron sheath derived from photoemission laboratory measurements. *Journal of Geophysical Research (1896-1977)*, *78*(16), 2885–2906. https://doi.org/10.1029/JA078i016p02885

Guillemant, S., Génot, V., Matéo-Vélez, J.-C., Ergun, R., & Louarn, P. (2012). Solar wind plasma interaction with solar probe plus spacecraft. *Annales Geophysicae*, *30*(7), 1075–1092. https://doi.org/10.5194/angeo-30-1075-2012

Guillemant, S., Maksimovic, M., Hilgers, A., Pantellini, F., Lamy, L., Louarn, P., et al. (2017). A study of Solar Orbiter spacecraft–plasma interactions effects on electric field and particle measurements. *IEEE Transactions on Plasma Science*, *45*(9), 2578–2587. https://doi.org/10.1109/TPS.2017.2731054

Halekas, J. S., Whittlesey, P., Larson, D. E., McGinnis, D., Maksimovic, M., Berthomier, M., et al. (2020). Electrons in the young solar wind: First results from the Parker Solar Probe. *The Astrophysical Journal - Supplement Series*, *246*(2), 22. https://doi.org/10.3847/1538-4365/ab4cec

Holmberg, M. K. G., Cipriani, F., Nilsson, T., Hess, S., Huybrighs, H. L. F., Hadid, L. Z., et al. (2021). Cassini-plasma interaction simulations revealing the Cassini ion wake characteristics: Implications for in-situ data analyses and ion temperature estimates. *Journal of Geophysical Research: Space Physics*, *126*(8), e2020JA029026. https://doi.org/10.1029/2020JA029026

Holmberg, M. K. G., Shebanits, O., Wahlund, J.-E., Morooka, M. W., Vigren, E., André, N., et al. (2017). Density structures, dynamics, and seasonal and solar cycle modulations of Saturn's inner plasma disk. *Journal of Geophysical Research: Space Physics*, *122*(12), 12258–12273. https://doi.org/10.1002/2017JA024311

Holmberg, M. K. G., Wahlund, J.-E., Morooka, M. W., & Persoon, A. M. (2012). Ion densities and velocities in the inner plasma torus of Saturn. *Planetary and Space Science*, *73*(1), 151–160. https://doi.org/10.1016/j.pss.2012.09.016

Huebner, W., & Mukherjee, J. (2015). Photoionization and photodissociation rates in solar and blackbody radiation fields. *Planetary and Space Science*, *106*, 11–45. https://doi.org/10.1016/j.pss.2014.11.022

JUICE Operational SPICE Kernel Dataset. (2024). ESA SPICE service [Dataset]. European Space Agency. https://doi.org/10.5270/esa-ybmj68p

Kilpua, E., Koskinen, H. E. J., & Pulkkinen, T. I. (2017). Coronal mass ejections and their sheath regions in interplanetary space. *Living Reviews in Solar Physics*, *14*(1), 5. https://doi.org/10.1007/s41116-017-0009-6

Lazar, M., Pierrard, V., Poedts, S., & Fichtner, H. (2020). Characteristics of solar wind suprathermal halo electrons. *Astronomy & Astrophysics*, *642*, A130. https://doi.org/10.1051/0004-6361/202038830

Maksimovic, M., Zouganelis, I., Chaufray, J.-Y., Issautier, K., Scime, E. E., Littleton, J. E., et al. (2005). Radial evolution of the electron distribution functions in the fast solar wind between 0.3 and 1.5 AU. *Journal of Geophysical Research*, *110*(A09104). https://doi.org/10.1029/2005JA011119

Michotte de Welle, B., Aunai, N., Nguyen, G., Lavraud, B., Génot, V., Jeandet, A., & Smets, R. (2022). Global three-dimensional draping of magnetic field lines in Earth's magnetosheath from in-situ spacecraft measurements. *Journal of Geophysical Research: Space Physics*, *127*(12), e2022JA030996. https://doi.org/10.1029/2022JA030996

Newbury, J. A., Russell, C. T., Phillips, J. L., & Gary, S. P. (1998). Electron temperature in the ambient solar wind: Typical properties and a lower bound at 1 AU. *Journal of Geophysical Research*, *103*(A5), 9553–9566. https://doi.org/10.1029/98JA00067

Pierrard, V., Lazar, M., & Štverák, S. (2020). Solar wind plasma particles organized by the flow speed. *Solar Physics*, *295*(11), 151. https://doi.org/10.1007/s11207-020-01730-z

Sarrailh, P., Matéo-Vélez, J.-C., Hess, S. L. G., Roussel, J.-F., Thiébault, B., Forest, J., et al. (2015). SPIS 5: New modeling capabilities and methods for scientific missions. *IEEE Transactions on Plasma Science*, *43*(9), 2789–2798. https://doi.org/10.1109/TPS.2015.2445384

Schläppi, B., Altwegg, K., Balsiger, H., Hässig, M., Jäckel, A., Wurz, P., et al. (2010). Influence of spacecraft outgassing on the exploration of tenuous atmospheres with in situ mass spectrometry. *Journal of Geophysical Research*, *115*(A12). https://doi.org/10.1029/2010JA015734

Sjögren, A., Eriksson, A. I., & Cully, C. M. (2012). Simulation of potential measurements around a photoemitting spacecraft in a flowing plasma. *IEEE Transactions on Plasma Science*, *40*(4), 1257–1261. https://doi.org/10.1109/TPS.2012.2186616

Spacecraft Plasma Interaction Software [Software]. (2024). Spacecraft plasma interactions network in Europe. Retrieved from https://www.spis.org/software/spis/get/

Štverák, Š., Maksimovic, M., Trávníček, P. M., Marsch, E., Fazakerley, A. N., & Scime, E. E. (2009). Radial evolution of nonthermal electron populations in the low-latitude solar wind: Helios, Cluster, and Ulysses observations. *Journal of Geophysical Research*, *114*(A5). https://doi.org/10.1029/2008JA013883

Venzmer, M. S., & Bothmer, V. (2018). Solar-wind predictions for the Parker Solar Probe orbit - Near-Sun extrapolations derived from an empirical solar-wind model based on Helios and OMNI observations. *Astronomy & Astrophysics*, *611*, A36. https://doi.org/10.1051/0004-6361/201731831

Wahlund, J.-E., Bergman, J. E. S., Åhlén, L., Puccio, W., Cecconi, B., Kasaba, Y., et al. (2024). The Radio and Plasma Wave Investigation (RPWI) for the Jupiter Icy Moons Explorer (JUICE). *Space Science Reviews*, in press.

Wang, X., Hsu, H.-W., & Horányi, M. (2015). Identification of when a Langmuir probe is in the sheath of a spacecraft: The effects of secondary electron emission from the probe. *Journal of Geophysical Research: Space Physics*, *120*(4), 2428–2437. https://doi.org/10.1002/2014JA020624

Wilson, L. B. III, Stevens, M. L., Kasper, J. C., Klein, K. G., Maruca, B. A., Bale, S. D., et al. (2018). The statistical properties of solar wind temperature parameters near 1 AU. *The Astrophysical Journal - Supplement Series*, *236*(2), 41. https://doi.org/10.3847/1538-4365/aab71c